

FourierSR: A Fourier Token-based Plugin for Efficient Image Super-Resolution

Wenjie Li, Heng Guo*, Yuefeng Hou, and Zhanyu Ma

Abstract—Image super-resolution (SR) aims to recover low-resolution images to high-resolution images, where improving SR efficiency is a high-profile challenge. However, commonly used units in SR, like convolutions and window-based Transformers, have limited receptive fields, making it challenging to apply them to improve SR under extremely limited computational cost. To address this issue, inspired by modeling convolution theorem through token mix, we propose a Fourier token-based plugin called FourierSR to improve SR uniformly, which avoids the instability or inefficiency of existing token mix technologies when applied as plug-ins. Furthermore, compared to convolutions and windows-based Transformers, our FourierSR only utilizes Fourier transform and multiplication operations, greatly reducing complexity while having global receptive fields. Experiments show that our FourierSR as a plugin brings an average PSNR gain of 0.34dB for existing efficient SR methods on Manga109 test set at the scale of $\times 4$, while the average increase in the number of Params and FLOPs is only 0.6% and 1.5% of original sizes. Code link: <https://github.com/PRIS-CV/FourierSR>.

Index Terms—A Plugin, Token Mix, Convolution Theorem, Global Receptive Field, Efficient Image Super-Resolution

I. INTRODUCTION

IMAGE super-resolution (SR) aims to reconstruct a low-resolution (LR) image to a high-resolution (HR) image, which plays an important role in computer vision, such as visual quality improvement [1] and security surveillance [2]. To promote the application of SR on devices with limited computational resources, efficient SR has been continuously studied. However, existing methods face a trade-off between performance and computational cost. Therefore, a plug-and-play unit with the ability to efficiently enhance performance while consuming minimal computational costs is desired.

The challenge of the plug-and-play unit for efficient SR lies in balancing complexity and performance. Existing CNN-based methods utilize techniques such as feature distillation [3] and wide activation [4] to reduce model complexity, of which 3×3 convolutions are widely used. However, compared to the local receptive fields from convolution, larger receptive fields are

This work was supported by Beijing-Tianjin-Hebei Basic Research Funding Program No. F2024502017, National Natural Science Foundation of China (Grant No. 62472044, U24B20155, 62225601, U23B2052), Hebei Natural Science Foundation Project No. 242Q0101Z, Beijing Natural Science Foundation Project No. L242025, and in part by the Fundamental Research Funds for the Beijing University of Posts and Telecommunications under Grant 2025AI4S15. (*: Corresponding author)

Wenjie Li, Heng Guo, and Zhanyu Ma are with the Pattern Recognition and Intelligent System Laboratory, School of Artificial Intelligence, Beijing University of Posts and Telecommunications (BUPT), Beijing 100080, China (e-mail: {cswjli, guoheng, mazhanyu}@bupt.edu.cn).

Yuefeng Hou is with the School of Microelectronics, Tianjin University (TJU), Tianjin 300072, China (e-mail: houyuefeng@tju.edu.cn).

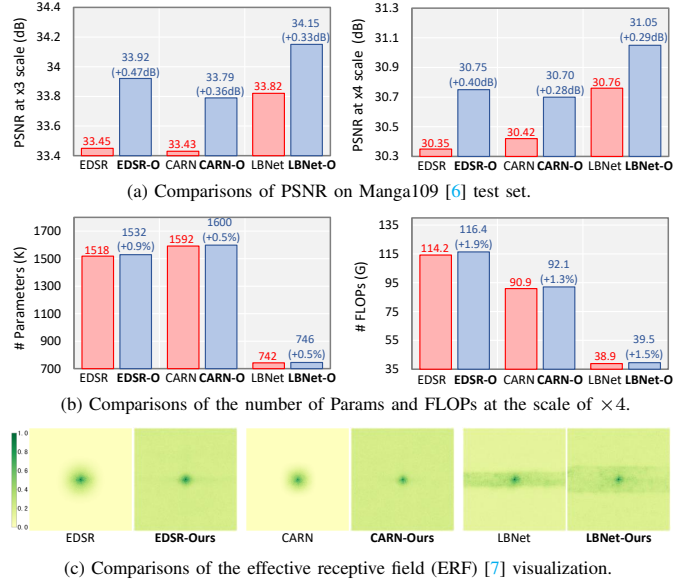


Figure 1: **(Top)** The performance and efficiency improvement embedded with our FourierSR (-O), a plugin for improving existing efficient SR methods [8]–[10]. **(Bottom)** With our FourierSR plugin, the receptive field of existing efficient SR methods [8]–[10] can be extended effectively.

preferred for improving the performance of SR. Transformer can be one solution for obtaining global receptive fields, but it also introduces high computational costs. Existing Transformer-based efficient SR methods [5] reduce the complexity by dividing inputs into small windows. Due to limited connections between different windows, the receptive field of models is limited. Therefore, this paper aims to design an efficient SR plugin with low costs and global receptive fields.

Inspired by performing token mixing in the Fourier domain to model global convolution via convolution theorem [11] at low costs in image recognition and detection tasks [12], token mix can be one solution for designing efficient SR plugins, where token mix refers to exchange information contained in divided features of inputs. Despite the potential of applying token mix techniques to SR tasks, it is non-trivial to apply the token mix in efficient SR plugins where expensive costs or instability could be introduced. For example, AFNO [13] utilizes a set of matrix multiplications to mix channel tokens in the Fourier domain, bringing computational costs to be too expensive for efficient SR. GFNet [14] defines global filters the same size as inputs to perform token mix. However, in the SR task, the input size differs between training and testing, making

it unstable to apply this approach consistently. AFFNet [15] multiplies mixed tokens with Fourier features. However, the multiplication of complex tensors produces unstable values, leading to gradient explosion in SR training.

To construct improved Fourier tokens suitable for the efficient SR plugin, we propose FourierSR to boost off-the-shelf efficient SR methods. Similar to existing token mix methods, we simulate the global convolution based on the convolution theorem [11], which states that element-wise products in the frequency domain are equivalent to convolutions in the time domain. The key difference is that we find using defined local kernels to perform token mixing on the real and imaginary parts of Fourier features results in more robust and superior performance. Specifically, we extend defined local kernels to obtain simulated global kernels, which allows FourierSR to avoid the size inconsistency caused by defining global filters as kernels for SR training and testing in GFNet [14], and the gradient explosion resulting from defining Fourier features as kernels in AFFNet [15]. Furthermore, we demonstrate that multiplying the real and imaginary parts of Fourier features with defined filters further results in enhanced global receptive fields. Additionally, such operation is lightweight, avoiding the slow inference and large number of parameters associated with heavy computational operations in AFNO [16] and FFC [17].

Due to its global receptive field and its absence of heavy computational operations, our FourierSR is ideally suited as a plug-and-play unit to enhance efficient SR methods. Experiments show our FourierSR as a plugin can be easily adapted to off-the-shelf efficient methods and improve their performance while avoiding the significant gain of computational cost. As shown in Fig. 1 (a) and (b), our FourierSR improves PSNR by more than 0.34dB while increasing the average number of parameters by only 0.6% and FLOPs by only 1.5%, which benefits from our FourierSR’s ability to expand the limited receptive field significantly of existing efficient CNN [8], [9] and windows-based Transformer [10] methods, as shown in Fig. 1 (c). Our contributions can be summarized as:

- We propose a plugin called FourierSR, which improves off-the-shelf efficient SR by simulating global convolution based on the token mix and convolution theorem.
- We propose a token mix scheme that uses local filters to modulate real and imaginary parts of Fourier features, efficiently and robustly achieving global receptive fields.
- Experiments show FourierSR can be a plug-and-play unit that efficiently expands receptive fields of existing methods and thus improves SR quality with minimal costs.

II. RELATED WORK

A. Efficient SR Methods

To reduce the high computational costs of general SR methods [18]–[22], efficient SR has been developed recently. CARN [9] utilizes group convolution and recursive mechanisms to save SR costs. s-LWSR [23] designs a lightweight network with a U-shaped backbone plus depth-separable convolution. IDN [24] introduces the concept of information distillation to improve model speed while maintaining model performance. Subsequently, RFDN [25], FDIWN [4], and FIWHN [26]

Table I: Existing methods based on Fourier or token-mix, while capable of simulating non-local convolutions, are not suitable as plug-ins due to their poor stability or computational inefficiency.

Strategy	Methods	Why isn’t suitable as plug-ins?
Conducting convolution in the Fourier domain	[17], [30], <i>etc</i>	Convolutions or linear layers are computational inefficiency.
Defining global filters for token mix	[16], [31], <i>etc</i>	Different size in train and test, large number of Params.
Utilizing Fourier features for token mix	[32], [15], [33], <i>etc</i>	Prone to gradient explosions during training.
A lot of matrix mul in the Fourier domain	[12], [13], [34], <i>etc</i>	Slow inference speed.
windows-based mul in the Fourier domain	[32], <i>etc</i>	Limited ability of model representation

further enhance the model’s representation ability by improved information distillation. To obtain a larger receptive field, ShuffleMixer [27] and CFSR [28] utilize separable large kernel convolution to efficiently model a wide range of receptive fields with minimal costs. SMFANet [29] further aggregates local and non-local features from large kernel convolution to compress models while improving SR performance. However, CNN-based SR methods still face the dilemma that it is difficult to further improve SR due to their limited receptive fields.

To explore the global receptive field of models, SwinIR [5] first introduces the windows-based Transformer to capture long-range features. Then, A series of Transformer-based methods for efficient SR have been proposed. Specifically, ESRT [35] and LBNNet [10] split the vectors in the Transformer to reduce the costs of the Transformer. ELAN [36] speeds up the Transformer’s inference through self-attention share mechanisms. Onni-SR [37], WFEN [38], and DMNet [39] enhance the ability of the Transformer to extract features by expanding the range of pixel modeling. CFIN [40] improves the cross-scale interaction and contextual reasoning ability of the Transformer. NGSwin [41] attempts to solve the problem of difficulty in connecting information from different windows in the Transformer. SRFormer [42] improves SR by permutation spatial information to channels. To reduce the complexity of the Transformer, MambaIR [43] first introduces the state space model to achieve long-range modeling with linear complexity. Unlike these methods that design complete networks, our method simulates global convolution by improved token mix in the Fourier domain, which can be an SR plugin to improve off-the-shelf efficient SR methods with minimal costs.

B. Fourier-based and Token Mix-based Methods

Fourier-based Methods. Fourier-based methods have grown significantly due to Fourier information can be used to improve the performance of models from a frequency analysis perspective. Specifically, in low-level tasks, NL-FFC [30] conducts convolutions in the Fourier domain to explore the relationship of frequency features. SFMNet [44] explores the frequency-spatial connections between the Fourier domain and spatial domain. FECNet [45], FSDGN [46], FourLLIE [47], and FourierDiff [48] achieve precise restoration of image

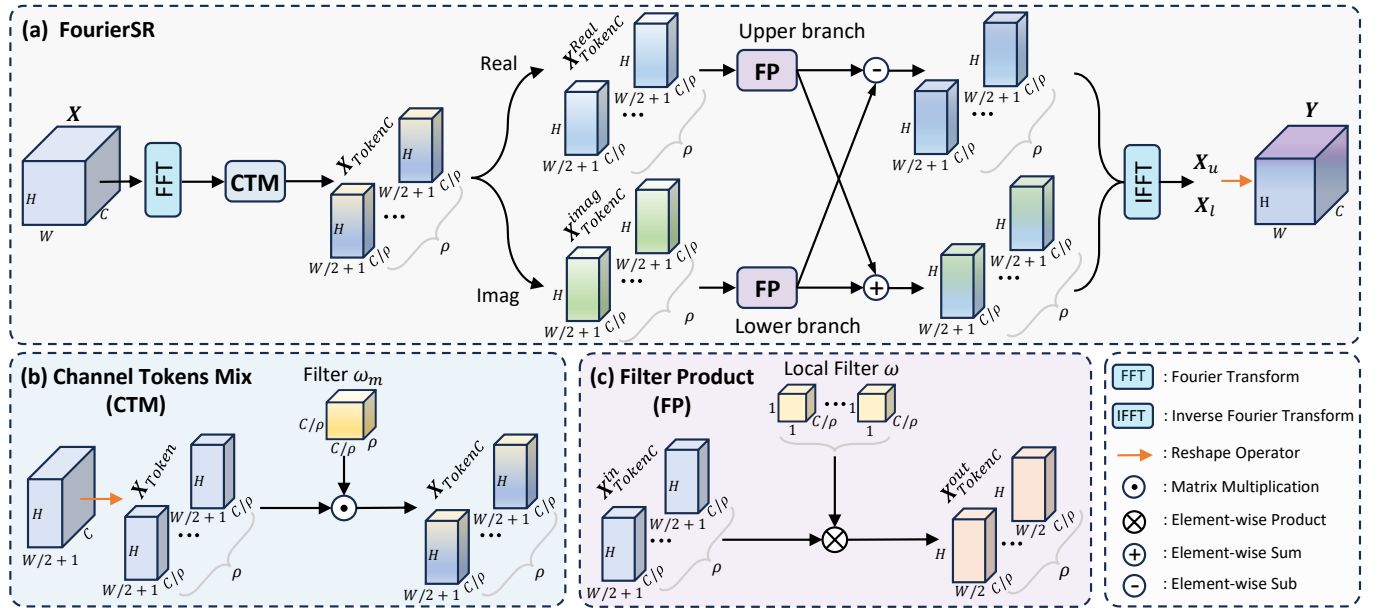


Figure 2: Overview of (a) FourierSR, (b) Channel Tokens Mix (CTM) in FourierSR, (c) Filter Product (FP) in FourierSR.

backgrounds by accurately reconstructing the amplitude and phase in the Fourier domain, enabling tasks such as defogging, low-light enhancement, and more. FreqMamba [49] improves the efficiency of models by connecting them to the Fourier transform for global degradation modeling. However, these methods utilize feature extraction modules in the Fourier domain, which is parametrically inefficient as plug-ins.

Token Mix-based Methods. Token mix-based methods have recently been introduced in high-level tasks, such as image recognition and detection task [12], for exploring long-range features with less complexity. Specifically, FFC [17] enhances representations through element-by-element addition and convolutions in the Fourier domain. GFNet [16] and DFFormer [31] explore global features by element-wise multiplication with global learnable filters. AFFNet [15] performs semantic analysis in the Fourier domain to model large kernel convolution. FNO [12], AFNO [13], and FourierGNN [34] simulate the global convolution through the matrix multiplication with learnable filters. However, as shown in the TABLE I, the above Fourier-based or token-based methods are non-trivial in applying efficient SR due to their stability and efficiency. In this paper, we enhance off-the-shelf efficient SR methods with our improved Fourier tokens that apply to efficient SR.

III. METHOD

In this section, we first introduce preliminary knowledge, including token mix and the convolution theorem [11] in Section III-A. Then, we introduce our FourierSR based on the above knowledge in Section III-B. Next, we analyze our strengths compared with related methods in Section III-C. Finally, we introduce the location of our FourierSR insertion within existing efficient SR methods in Section III-D.

A. Preliminary Knowledge

Our work aims to design a computationally efficient plugin with global receptive fields by token mix and convolution

theorem. We will introduce the above concepts below.

1) *Token Mix:* Token mix has received attention for learning non-local features in high-level tasks. Before introducing the token mix, we first describe what a token is. For a feature tensor $\mathbf{X} \in \mathbb{R}^{H \times W \times C}$, where H, W, C is height, width, and channel counts, respectively. This feature can be viewed as obtained by transforming a series of tokens \mathbf{x} , where the shape of a token can be $\mathbb{R}^{H \times W \times (C/\rho) \times \rho}$, $\mathbb{R}^{(H/\rho) \times \rho \times (W/\rho) \times \rho \times C}$, or $\mathbb{R}^{(H/\rho) \times \rho \times (W/\rho) \times \rho \times (C/\rho) \times \rho}$ etc, where ρ is the number of tokens in the H, W or C dimension. On this basis, the process of mixing non-local features of original tokens \mathbf{x} to get updated tokens \mathbf{x}^u can be described:

$$\mathbf{x}^u = \sum_{i \in \mathcal{N}(\mathbf{x})} \omega^{i \rightarrow u} \odot \phi(\mathbf{x}^i), \quad (1)$$

where $\mathcal{N}(\mathbf{x})$ are token features of one or more dimensions of \mathbf{x} , \mathbf{x}^i is a token in $\mathcal{N}(\mathbf{x})$. $\omega^{i \rightarrow u}$ is the weight exchange or mix, \odot is the matrix multiplication or element-wise product operator. ϕ is the feature embedding function.

2) *Convolution Theorem:* The time domain convolution theorem [11], in which convolutions in the time domain correspond to element-wise products in the frequency domain. This theorem can be formulated as:

$$\mathcal{F}[g(t) * h(t)] = \mathcal{F}[g(t)] \times \mathcal{F}[h(t)], \quad (2)$$

where \mathcal{F} is the Fourier transform, $g(t)$ and $h(t)$ are time domain signals, \times is a element-wise product, $*$ is a convolution. Next, we introduce some properties of the convolution theorem that will be used below. For a tensor \mathbf{X} , there are:

$$\mathcal{T}[\mathcal{F}(\mathbf{X})] = \mathcal{F}(\hat{\mathbf{X}}), \hat{\mathbf{X}} = \delta(\mathbf{X}), \quad (3)$$

$$\mathcal{F}^{-1}[\mathcal{F}(\mathbf{X} \pm \hat{\mathbf{X}})] = \mathcal{F}^{-1}[\mathcal{F}(\mathbf{X})] \pm \mathcal{F}^{-1}[\mathcal{F}(\hat{\mathbf{X}})], \quad (4)$$

$$\mathcal{F}^{-1}\{\mathcal{F}[g(t)] \times \mathcal{F}[h(t)]\} = g(t) * h(t), \quad (5)$$

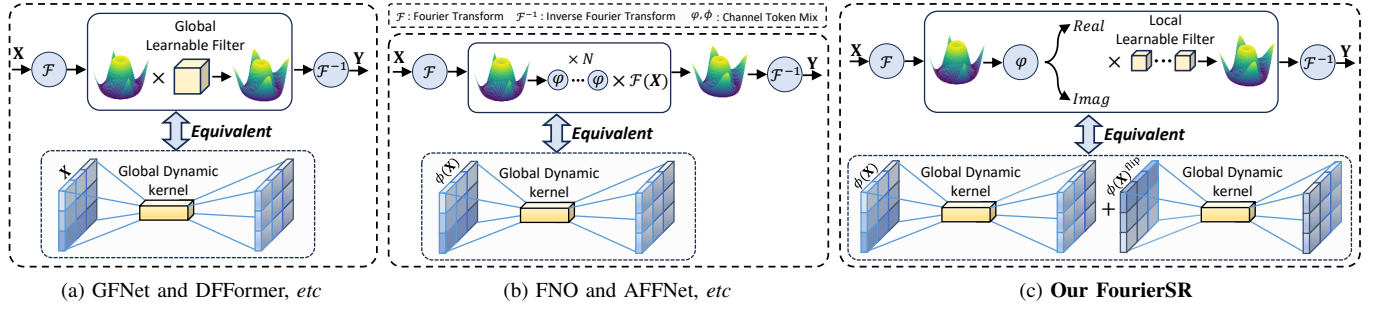


Figure 3: Comparisons of our FourierSR and existing Fourier token-based methods. (a) GFNet [16] and DFFormer [31] directly define global filters with the same size as inputs as kernels to simulate global convolutions. (b) FNO [12], FFTformer [32] and AFFNet [15] use N ($N \geq 8$) matrix multiplications for channel mix or define Fourier features as kernels to simulate global convolutions. (c) Our FourierSR extends local filters to global as global kernels to multiply with real and imaginary parts of Fourier features, which is equivalent to global convolutions of an input tensor plus its flipped.

where \mathcal{F}^{-1} is an inverse Fourier transform, \mathcal{T} is a series of transformations, \hat{X} is obtained after not changing the tensor size token mix δ on X . In addition, for the real and imaginary parts of Fourier features, according to deformations of the convolution theorem, there are:

$$\mathcal{F}^{-1}[\text{Real}(\mathcal{F}(X))] = \frac{1}{2}X + \frac{1}{2}X^{flip}, \quad (6)$$

$$\mathcal{F}^{-1}[\text{Imag}(\mathcal{F}(X))] = \frac{1}{2}X - \frac{1}{2}X^{flip}, \quad (7)$$

where Real and Imag are real and imaginary parts of $\mathcal{F}(X)$, respectively. X^{flip} is the flip of tensor X .

B. FourierSR

This subsection aims to prove mathematically that our FourierSR is equivalent to global dynamic convolutions.

1) *Filter Product (FP)*: First, we need to describe **why local filters can be converted to global filters** during element products and with abilities to adjust network weights dynamically, which is crucial for proving that our FourierSR can be equated to global dynamic convolutions.

For a tensor $X_{TokenC}^{in} \in \mathbb{R}^{\rho, C/\rho, H, (W/2+1)}$ and a local filter $\omega \in \mathbb{R}^{\rho, C/\rho, 1, 1}$, as shown in Fig. 2 (b), when X_{TokenC}^{in} and ω do element-wise products, the broadcast mechanism of torch firstly expands ω into a global filter of the same size as X_{TokenC}^{in} . Then, ω as a learnable parameter can convert X_{TokenC}^{in} into a learnable parameter to manage its weight optimization during training dynamically. Meanwhile, the number of params of this filter is still equal to the local filter rather than the global filter. The process of broadcast mechanism and obtaining $X_{TokenC}^{in} \in \mathbb{R}^{\rho, C/\rho, H, (W/2+1)}$ with dynamical weights is:

$$\omega \in \mathbb{R}^{\rho, C/\rho, 1, 1} \rightarrow \omega \in \mathbb{R}^{\rho, C/\rho, H, (W/2+1)}, \quad (8)$$

$$X_{TokenC}^{out} = \omega \in \mathbb{R}^{\rho, C/\rho, H, (W/2+1)} \times X_{TokenC}^{in}, \quad (9)$$

therefore, local filters with light computational costs can be viewed as global filters in FP and make networks capable of adjusting weights dynamically in our FourierSR. Next, we will prove that our FourierSR is equal to the global dynamic convolution based on this.

Table II: Complexity comparison between convolution (Conv), windows-based Transformer (WTrans) [14], existing token mix-based methods, *i.e.*, FFC [17], GFNet [16], AFNO [13], AFFNet [15], and our FourierSR. Our method has the smallest Params counts and the second smallest FLOPs counts. k : Convolution kernel size. C : The number of input and output channels. H, W : Height and width of input images. M : windows size in W-Trans. ρ : Tokens counts.

Methods	FLOPs	Parameters
Conv	$k^2 C^2 H W$	$k^2 C^2$
WTrans [14]	$4C^2 H W + 2M^2 C H W$	$4C^2$
FFC [17]	$k^2 C^2 H W + 2C H W \log_2 H W$	$k^2 C^2$
GFNet [16]	$C H W + 2C H W \log_2 H W$	$C H W$
AFNO [13]	$8C^2 H W / \rho + 2C H W \log_2 H W$	$(1 + 4/\rho)C^2 + 4C$
AFFNet [15]	$8C^2 H W / \rho + 2C H W \log_2 H W$	$(1 + 4/\rho)C^2 + 4C$
Ours	$C^2 H W / \rho + 2C H W \log_2 H W$	$(6 + \rho)C$

2) *Mathematical Proof*: As shown in Fig. 2 (a), for an input tensor $X \in \mathbb{R}^{C \times H \times W}$, we first perform the Fourier transform on X and then utilize a reshape operator as the feature embedding unit ϕ to get Fourier tokens $X_{Token} \in \mathbb{R}^{\rho, C/\rho, H, (W/2+1)}$. Next, we perform the channel tokens mix using matrix multiplication with our defined complex filter $\omega_m \in \mathbb{R}^{\rho, C/\rho, C/\rho}$ to get a channel-mixed token X_{TokenC} . Combined with Eq.(3), this process can be described and equated as:

$$X_{TokenC} = \omega_m \odot \phi(\mathcal{F}(X)) = \mathcal{F}(\hat{X}), \quad (10)$$

where $\hat{X} = \delta(X)$, $\hat{X} \in \mathbb{R}^{\rho, C/\rho, H, (W/2+1)}$, δ is a random channel token mix, \odot is a matrix multiplication operator, \mathcal{F} and \mathcal{F}^{-1} have same meaning with Eq.(3). Then, we perform the spatial token mix on height and width dimensions using our defined local filter ω . For the upper branch in Fig. 2 (a), combined with Eq.(4), the output X_u can be described and equated as:

$$\begin{aligned} X_u &= \mathcal{F}^{-1}[\omega \times \text{Real}(\mathcal{F}(\hat{X})) - \omega \times \text{Imag}(\mathcal{F}(\hat{X}))] \\ &= \mathcal{F}^{-1}[\omega \times \text{Real}(\mathcal{F}(\hat{X}))] - \mathcal{F}^{-1}[\omega \times \text{Imag}(\mathcal{F}(\hat{X}))] \end{aligned} \quad (11)$$

combined with Eq.(8), the size of $\omega \in \mathbb{R}^{\rho, C/\rho, 1, 1}$ at this moment after broadcasting is same as $\text{Real}(\mathcal{F}(\hat{X}))$,

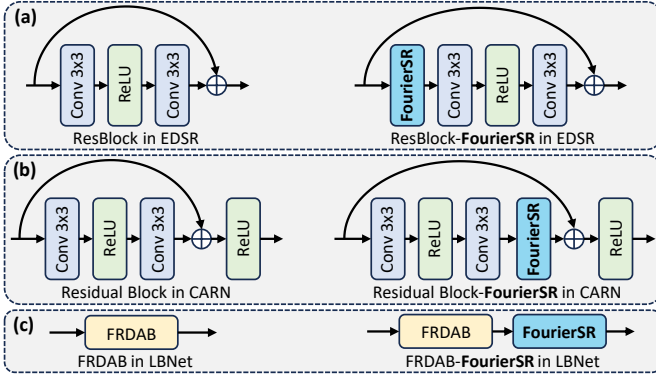


Figure 4: Overview of positions where our FourierSR is inserted into methods listed in TABLE III. (a): EDSR [8] and EDSR-Ours, (b): CARN [9] and CARN-Ours, (c): LBNNet [10] and LBNNet-Ours.

$Imag(\mathcal{F}(\hat{X}))$, and $\mathcal{F}(\hat{X}) \in \mathbb{R}^{\rho, C/\rho, H, (W/2+1)}$. Then, combined with Eq.(5), X_u can be further described as:

$$X_u = \mathcal{F}^{-1}(\omega) * \mathcal{F}^{-1} \left[Real(\mathcal{F}(\hat{X})) \right] - \mathcal{F}^{-1}(\omega) * \mathcal{F}^{-1} \left[Imag(\mathcal{F}(\hat{X})) \right], \quad (12)$$

combined with Eq.(6) and Eq.(7), we have:

$$X_u = \mathcal{F}^{-1}(\omega) * \left[\frac{\hat{X}}{2} + \frac{\hat{X}^{flip}}{2} \right] - \mathcal{F}^{-1}(\omega) * \left[\frac{\hat{X}}{2} - \frac{\hat{X}^{flip}}{2} \right], \quad (13)$$

since convolutions satisfy the distributive law, the above equation can be equated to:

$$X_u = \mathcal{F}^{-1}(\omega) * \left[\frac{\hat{X}}{2} + \frac{\hat{X}^{flip}}{2} - \frac{\hat{X}}{2} + \frac{\hat{X}^{flip}}{2} \right] = \mathcal{F}^{-1}(\omega) * \hat{X}^{flip}, \quad (14)$$

since ω is extended on spatial dimensions of the broadcast mechanism, the ω now has the same size with $\mathcal{F}(\hat{X})$ and $\mathcal{F}(\hat{X}^{flip})$, $\mathcal{F}^{-1}(\omega)$ has the same size with \hat{X} , $\hat{X}^{flip} \in \mathbb{R}^{C \times H \times W}$, which can be viewed a convolution kernel with global receptive field. According to the description in Eq.(9), $\mathcal{F}^{-1}(\omega)$ can convert the tensor to a learnable parameter to dynamically adjust its weight. Therefore, $X_u \in \mathbb{R}^{C \times H \times W}$ can be viewed as the result obtained by utilizing a convolution with a global receptive field kernel.

Similarly, combined with Eq.(4), Eq.(5), Eq.(6), and Eq.(7), the output X_l of lower branch can be described as:

$$\begin{aligned} X_l &= \mathcal{F}^{-1} \left[\omega \times Real(\mathcal{F}(\hat{X})) + \omega \times Imag(\mathcal{F}(\hat{X})) \right] \\ &= \dots \\ &= \mathcal{F}^{-1}(\omega) * \left[\frac{\hat{X}}{2} + \frac{\hat{X}^{flip}}{2} + \frac{\hat{X}}{2} - \frac{\hat{X}^{flip}}{2} \right] \\ &= \mathcal{F}^{-1}(\omega) * \hat{X}, \end{aligned} \quad (15)$$

similar with X_u in Eq.(14), $\mathcal{F}^{-1}(\omega)$ now has the same size with $\hat{X} \in \mathbb{R}^{C \times H \times W}$, $X_l \in \mathbb{R}^{C \times H \times W}$ can be viewed as the result obtained by a global convolution to \hat{X} . Filters ω are share-weighted with the upper branch. Finally, X_u and X_l obtained from the upper and lower branches are fused and

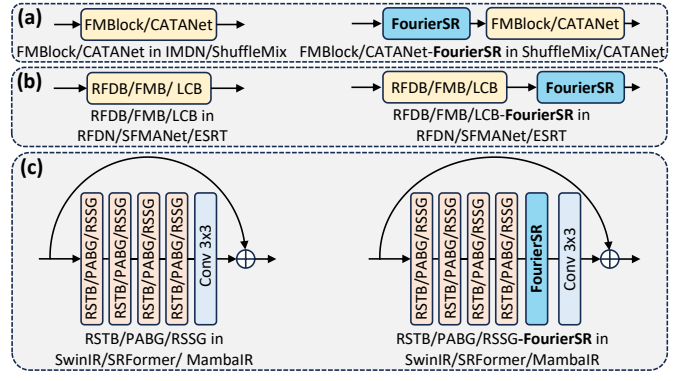


Figure 5: Overview of positions where our FourierSR is inserted into methods listed in Fig 6. (a): ShuffleMixer [27], CATANet [50] and (ShuffleMixer, CATANet)-Ours, (b): RFDN [25], SMFANet [29], ESRT [35] and (RFDN, SMFANet, ESRT)-Ours, (c): SwinIR [5], SRFormer [42], MambaIR [43] and (SwinIR, SRFormer, MambaIR)-Ours.

reshaped to get the final output Y . Since \hat{X} and \hat{X}^{flip} are obtained by channel token mix, the final result Y can be regarded as obtained by token mix of channel features plus convolution with a global receptive field kernel on inputs after data enhancement, leading our FourierSR with a strong ability to capture long-range features interaction.

C. Analysis of Strengths of Our FourierSR

1) *Structure Analysis*: As shown in Fig. 3, compared with one class of methods represented by GFNet [16] and DFFormer [31] in Fig. 3 (a), FourierSR shown in Fig. 3 (c) additionally does one mix for channel tokens and deals with real and imaginary parts of Fourier features, which allows models to obtain a better representation ability. Specifically, the channel token mix facilitates our model to exchange information in different groups of channels. Processing real and imaginary parts of Fourier features separately is equivalent to data enhancement. Due to the inconsistency of tensor sizes between SR training and testing, global filters can only be defined in the forward process, which seriously reduces model speed. In contrast, using broadcast mechanisms to extend local filters to global filters is more flexible. Another class of methods represented by AFNO [13] and AFFNet [15] in Fig. 3 (b) does too many mixes of channel tokens, resulting in huge costs and slow inference that do not apply to efficient SR. For AFFNet [15], its operation of using a Fourier tensor as a global kernel tends to cause divergence in the training of SR tasks.

2) *Complexity Comparison*: We give a complexity comparison in TABLE II. Regarding the number of FLOPs, our method is smaller than the windows-based Transformer (W-Trans), FFC [17], AFNO [13], and AFFNet [15]. The comparison of FourierSR with convolution can be simplified to a comparison of the number of k^2C and $C/\rho + 2\log_2 HW$. In SR, The height H and width W of the image are typically 1280/ s , 720/ s , where s is the scale factor. The kernel size in convolutions is typically 3. Therefore, our number of FLOPs is smaller than convolutions. Compared to GFNet [16], although

Table III: Quantitative evaluation of our method and existing efficient SR methods, where FLOPs is calculated on an upsampled image with a spatial size of 1280×720. The best results are emphasized in **bold**.

Scale	Methods	Params↓	FLOPs↓	Set5 [51]	Set14 [52]	BSDS100 [53]	Urban100 [54]	Manga109 [6]
				PSNR/SSIM	PSNR/SSIM	PSNR/SSIM	PSNR/SSIM	PSNR/SSIM
× 2	EDSR [8]	1370K	316.2G	37.99/0.9604	33.59/0.9175	32.16/0.8994	31.98/0.9272	38.55/0.9769
	EDSR-Ours	1384K	326.5G	38.07/0.9608	33.66/0.9182	32.19/0.8998	32.27/0.9290	38.89/0.9775
	Gain	+14K (1.0%)	+10.3G (3.3%)	+0.08/0.0004	+0.07/0.0007	+0.03/0.0004	+0.29/0.0018	+0.34/0.0006
	CARN [9]	1592K	222.8G	37.76/0.9590	33.52/0.9166	32.09/0.8978	31.92/0.9256	38.36/0.9765
	CARN-Ours	1600K	228.6G	38.03/0.9605	33.65/0.9179	32.15/0.8993	32.10/0.9276	38.74/0.9771
	Gain	+8K (0.5%)	+5.8G (2.6%)	+0.27/0.0015	+0.07/0.0013	+0.06/0.0015	+0.18/0.0020	+0.38/0.0006
	LBNNet [10]	731K	153.2G	38.05/0.9607	33.65/0.9177	32.16/0.8994	32.30/0.9291	38.88/0.9775
	LBNNet-Ours	735K	155.8G	38.13/0.9611	33.86/0.9194	32.21/0.9001	32.58/0.9311	39.08/0.9780
	Gain	+4K (0.5%)	+2.6G (1.7%)	+0.08/0.0004	+0.21/0.0017	+0.05/0.0007	+0.28/0.0020	+0.20/0.0005
× 3	EDSR [8]	1554K	160.4G	34.37/0.9270	30.28/0.8418	29.09/0.8052	28.15/0.8527	33.45/0.9439
	EDSR-Ours	1568K	164.7G	34.52/0.9279	30.39/0.8424	29.14/0.8058	28.36/0.8549	33.92/0.9460
	Gain	+14K (0.9%)	+4.3G (2.7%)	+0.15/0.0009	+0.11/0.0006	+0.05/0.0006	+0.21/0.0022	+0.47/0.0021
	CARN [9]	1592K	118.8G	34.29/0.9255	30.29/0.8407	29.06/0.8034	28.06/0.8493	33.43/0.9427
	CARN-Ours	1600K	121.2G	34.45/0.9277	30.42/0.8435	29.12/0.8059	28.33/0.8547	33.79/0.9454
	Gain	+8K (0.5%)	+2.4G (2.0%)	+0.16/0.0022	+0.13/0.0028	+0.06/0.0025	+0.27/0.0054	+0.36/0.0027
	LBNNet [10]	736K	68.4G	34.47/0.9277	30.38/0.8417	29.13/0.8061	28.42/0.8559	33.82/0.9460
	LBNNet-Ours	740K	69.4G	34.55/0.9283	30.47/0.8438	29.18/0.8074	28.66/0.8600	34.15/0.9477
	Gain	+4K (0.5%)	+1.0G (1.5%)	+0.08/0.0006	+0.09/0.0021	+0.05/0.0013	+0.24/0.0041	+0.33/0.0017
× 4	EDSR [8]	1518K	114.2G	32.09/0.8938	28.58/0.7813	27.57/0.7357	26.04/0.7849	30.35/0.9067
	EDSR-Ours	1532K	116.4G	32.30/0.8960	28.66/0.7826	27.63/0.7374	26.28/0.7899	30.75/0.9101
	Gain	+14K (0.9%)	+2.2G (1.9%)	+0.21/0.0022	+0.08/0.0013	+0.06/0.0007	+0.24/0.0050	+0.40/0.0034
	CARN [9]	1592K	90.9G	32.13/0.8937	28.60/0.7806	27.58/0.7349	26.07/0.7837	30.42/0.9070
	CARN-Ours	1600K	92.1G	32.18/0.8948	28.64/0.7825	27.62/0.7369	26.23/0.7875	30.70/0.9099
	Gain	+8K (0.5%)	+1.2G (1.3%)	+0.05/0.0011	+0.04/0.0019	+0.04/0.0020	+0.16/0.0028	+0.28/0.0029
	LBNNet [10]	742K	38.9G	32.29/0.8960	28.68/0.7832	27.62/0.7382	26.27/0.7906	30.76/0.9111
	LBNNet-Ours	746K	39.5G	32.36/0.8967	28.77/0.7846	27.69/0.7399	26.47/0.7947	31.05/0.9136
	Gain	+4K (0.5%)	+0.6G (1.5%)	+0.07/0.0007	+0.09/0.0006	+0.07/0.0017	+0.20/0.0039	+0.29/0.0025

we have a slightly higher number of FLOPs, this design contributes to enhancing the model’s representational capacity, including a channel tokens mix and an enhanced convolution range as shown in Fig. 3 (c). Moreover, FourierSR has the smallest number of parameters compared to convolutions, window-based Transformer, and existing token mix-based methods. Therefore, we can draw that our FourierSR is a computationally efficient plugin that is superior to common feature extraction modules and token mix methods.

D. Location of Our FourierSR Insertion

To highlight its generality, we randomly insert FourierSR into existing methods. As shown in Fig. 4, we provide a detailed illustration of the positions where FourierSR is inserted into methods listed in TABLE III. Similarly, as shown in Fig. 5, we randomly insert FourierSR into existing methods listed in Fig. 6. Overall, we do not intentionally choose the best location for the FourierSR to be inserted to emphasize the plug-and-play nature of FourierSR further. Our FourierSR can improve SR efficiency significantly regardless of where it is inserted and where the method belongs: CNN, Transformer, or Mamba.

IV. EXPERIMENTS

A. Datasets and Metrics

We use the first 800 images of DIV2K [61] as our training data and evaluate methods on five benchmarks, including

Table IV: Quantitative comparison of existing efficient SR methods empowered with ClassSR [55] framework and our FourierSR on Test2k [56], Test4k [56], and Test8K [56] test sets. Our method reduces complexity by reducing model depths.

Methods	Params↓	FLOPs↓	Speed↓	Test2K	Test4K	Test8K
				PSNR	PSNR	PSNR
FSRCNN [57]	25K	0.47G	0.9ms	25.61	26.90	32.66
FSRCNN-ClassSR [55]	113K	0.31G	5.3ms	25.61	26.91	32.73
FSRCNN-Ours	23K	0.30G	1.6ms	25.62	26.91	32.74
CARN-M [9]	295K	1.15G	9.1ms	25.95	27.34	33.18
CARN-M-ClassSR [55]	645K	0.82G	74.2ms	26.01	27.42	33.24
CARN-M-Ours	230K	0.80G	11.7ms	26.07	27.47	33.34
SRResNet [58]	1.5M	5.20G	11.8ms	26.19	27.65	33.50
SRResNet-ClassSR [55]	3.1M	3.62G	42.5ms	26.20	27.66	33.50
SRResNet-Ours	1.4M	3.03G	11.4ms	26.25	27.70	33.57

Set5 [51], Set14 [52], BSDS100 [53], Urban100 [54], and Manga109 [6]. To compare with ClassSR [55] fairly, we deal with DIV2K like ClassSR [55] to generate HR and LR training images. Meanwhile, we deal with DIV8K [56] to generate Test2K-8K test sets. As for evaluation metrics, we calculate PSNR and SSIM [62] on the Y channel in the YCbCr colour.

B. Implementation Details

We use the PyTorch framework with an NVIDIA GeForce RTX 4090 for all of the experiments. The learning rate, patch size, batch size, and optimizer settings are identical to the original methods. In the TABLE III, the number of

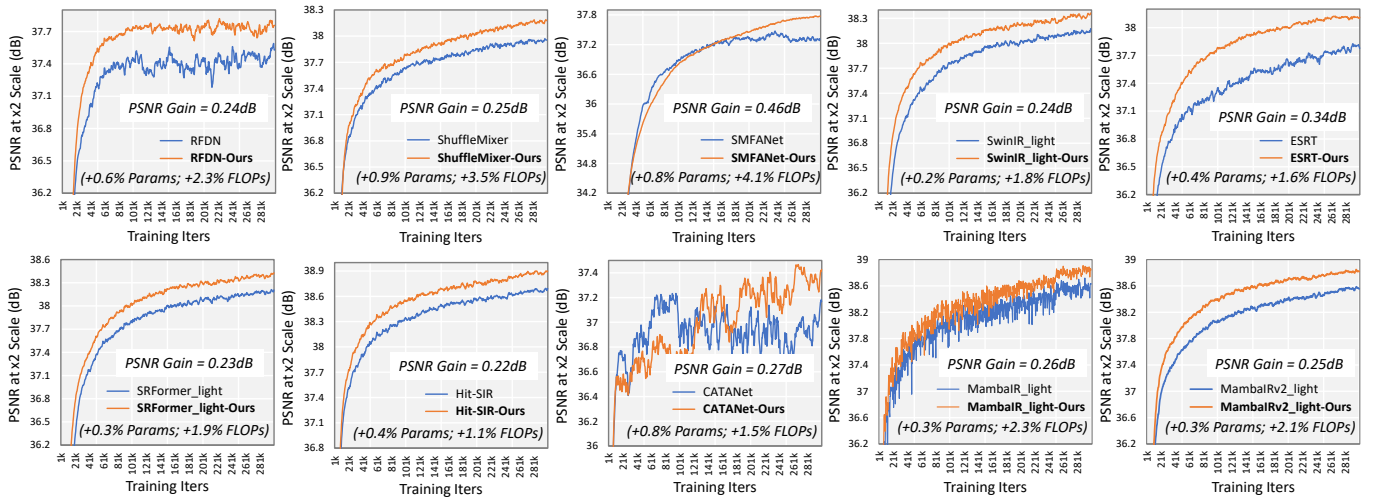


Figure 6: Comparison of PSNR in training between existing efficient methods and these methods empowered with FourierSR on Manga109 [6] test set. We choose CNN-based methods, *e.g.*, RFDN [25], ShuffleMixer [27], and SMFANet [29], Transformer-based methods, *e.g.*, SwinIR [5], ESRT [35], SRFormer [42], Hit-SIR [59], and CATANet [50], and Mamba-based method, *e.g.*, MambaIR [43] and MambaRv2 [60] as backbones. To speed up training, CNN-based and Mamba-based methods are trained with batch size=8 and patch size=32, and Transformer-based methods are trained with batch size=8 and patch size=16.

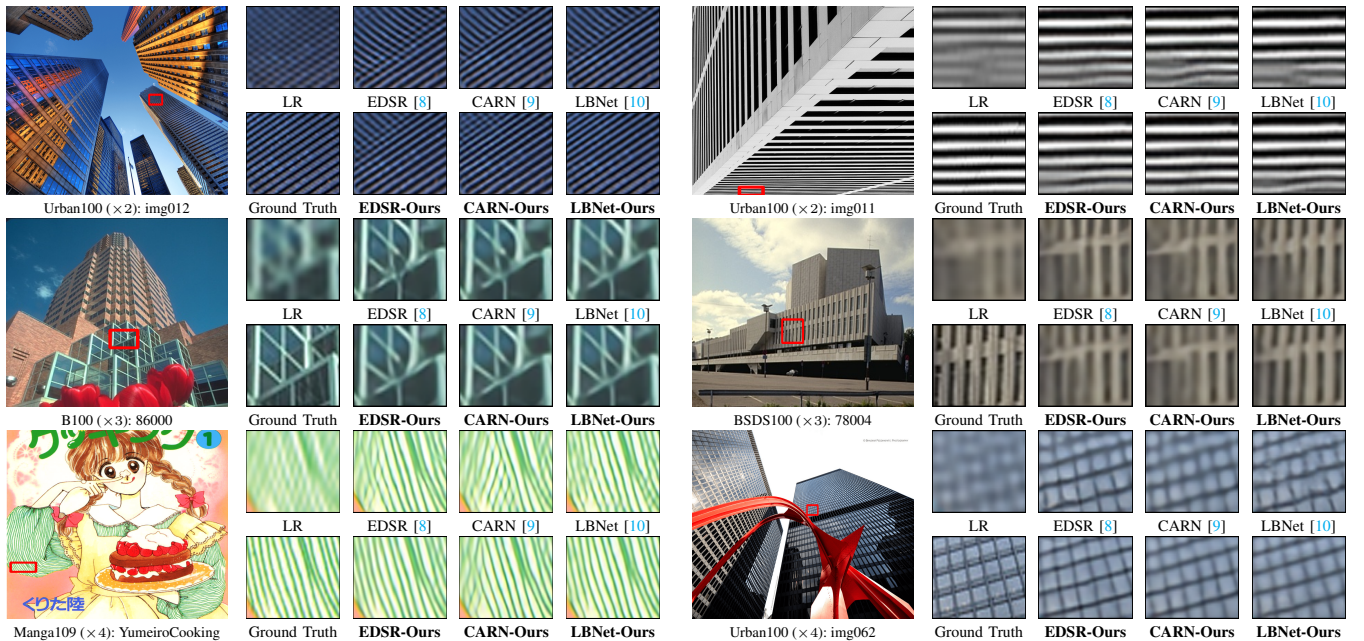


Figure 7: Qualitative comparisons between existing efficient SR methods and these methods empowered with our FourierSR.

our FourierSR is 16, 9, and 9 in EDSR [8], CARN [9], and LBNet [10], respectively. In the Fig. 6, the number of our FourierSR is 4, 5, 4, 6, 6, 6, 4, 8, 4 and 4 in RFDN [25], ShuffleMixer [27], SMFANet [29], SwinIR [5], ESRT [35], SRFormer [42], Hit-SIR [59], CATANet [50], MambaIR [43], and MambaRv2 [60]. The location where our FourierSR inserts into the existing methods network is random. Since FourierSR involves the computation of Fourier real and imaginary, to minimize errors that this part may cause, we introduce our Fourier Token Loss for supervision in our Supplementary Material. FLOPs and speed are measured corresponding to an HR image of the spatial size of 1280×720 pixels.

C. Benchmarks Evaluation

We choose existing efficient SR methods, including CNN-based methods, *e.g.*, EDSR [8], CARN [9], and Transformer-based methods, *e.g.*, LBNet [10], as benchmarks to evaluate our FourierSR's effectiveness. As shown in TABLE III, for existing methods, our FourierSR as a plug-and-play brings an average PSNR gain of 0.18 dB in five test sets, the average increase of Params and FLOPs counts of 0.6% and 2% of the original size. Furthermore, we compare the visual results of original benchmarks and benchmarks plus our FourierSR in Fig. 7. Due to the improved global ability of models after embedding our FourierSR, existing methods can handle a larger

Table V: Quantitative evaluation of a larger size version of existing methods listed in TABLE III and these methods empowered with our FourierSR. Our FourierSR demonstrates outstanding efficiency when applied in existing methods.

Scale	Methods	Params↓	FLOPs↓	Speed↓	Set5 [51]	Set14 [52]	BSDS100 [53]	Urban100 [54]	Manga109 [6]
					PSNR/SSIM	PSNR/SSIM	PSNR/SSIM	PSNR/SSIM	PSNR/SSIM
× 2	EDSR-L [8]	2552K	588.1G	52ms	38.03/0.9606	33.62/0.9177	32.18/0.8997	32.17/0.9288	38.69/0.9771
	EDSR-Ours	1384K	326.5G	58ms	38.07/0.9608	33.66/0.9182	32.19/0.8998	32.27/0.9290	38.89/0.9775
	CARN-L [9]	2368K	401.2G	51ms	37.83/0.9591	33.54/0.9168	32.10/0.8978	31.95/0.9259	38.45/0.9770
	CARN-Ours	1600K	228.6G	49ms	38.03/0.9605	33.65/0.9179	32.15/0.8993	32.10/0.9276	38.74/0.9771
	LBNet-L [10]	923K	193.7G	1465ms	38.07/0.9608	33.68/0.9180	32.17/0.8994	32.50/0.9301	38.97/0.9777
	LBNet-Ours	735K	155.8G	1204ms	38.13/0.9611	33.86/0.9194	32.21/0.9001	32.58/0.9311	39.08/0.9780

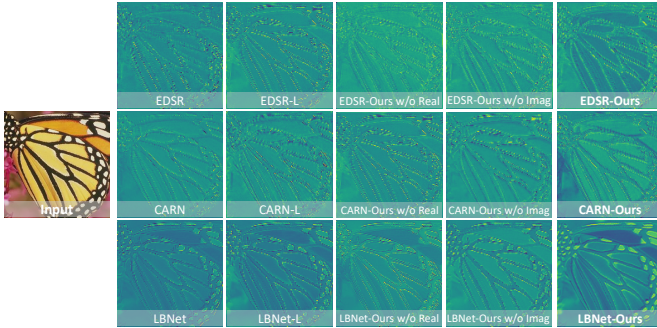


Figure 8: Visualization of feature maps at the same depth across different models, including a large-size version of existing methods and the upper (Real) and lower (Imag) branches of FourierSR. Our FourierSR enhances the model’s ability to capture comprehensive features.

range of features, as well as more subtle features. As a result, existing methods plus our FourierSR facilitate the correction of incorrectly recovered textures and the elimination of artifacts introduced by reconstruction. Since our method enhances the model’s ability to capture features by expanding its receptive field. Textures, due to their higher structures, benefit more from this enhancement and are thus more visibly improved. In contrast, other areas like details, may not show as pronounced a change because they tend to have tinier structures.

To further validate the generalization of our FourierSR, we test our FourierSR on more efficient SR methods, including CNN-based methods, *e.g.*, RFDN [25], ShuffleMix [27], SMFANet [29], Transformer-based methods, *e.g.*, SwinIR [5], ESRT [35], SRFormer [42], HiT-SIR [59], CATANet [50], and Mamba-based method, *e.g.*, MambaIR [43], MambaIRv2 [60] to further show FourierSR’s generalization. Due to GPU resource constraints, we train CNN-based and Mamba-based methods with batch size=8 and patch size=32 and Transformer-based methods with batch size=8 and patch size=16 to speed up training. As shown in Fig. 6, whether original methods are CNN-based, Transformer-based, or Mamba-based, FourierSR can be a plugin to significantly improve their performance with a tiny increase in computational costs. It is worth noting that for methods ShuffleMix [27] and SMFANet [29], which use extra Fourier-based loss, our FourierSR is equally effective in improving their performance by 0.25 dB and 0.46 dB, respectively. Evaluation of 13 efficient SR methods fully illustrates the generalizability of our FourierSR.

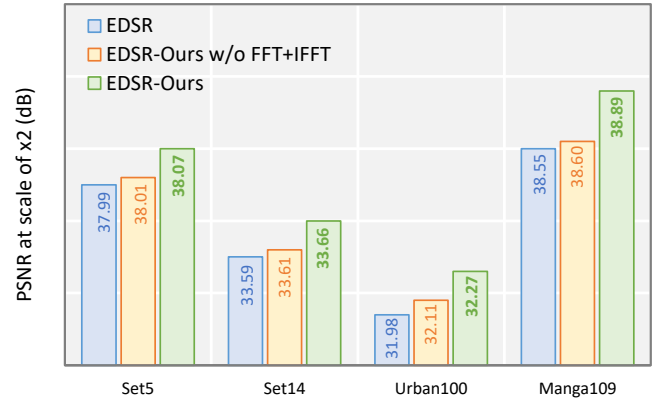


Figure 9: Ablation study on the theoretical validity of our FourierSR, where the convolution theorem no longer holds when Fourier transformers (FFT+IFFT) are not applied.

1) *Further Reduce Network Complexity*: Although our FourierSR expand the receptive field of models to improve SR, it still comes at the cost of a small increase in computational cost. To reduce the model computational cost, we can reduce the width or depth of existing methods to control network complexity further. In TABLE IV, we compare our FourierSR with a model accelerated framework called ClassSR [55]. For a fair comparison, our training and testing setting is the same as ClassSR framework. Our FourierSR performs better than ClassSR in terms of the number of Params and FLOPs, inference speed, and PSNR values. Specifically, our method improves SR performance while significantly reducing the computational costs of original SR methods. Additionally, it’s worth noting that ClassSR requires an increase in the number of Params of original methods by a factor of 2 to 4 to reduce the FLOPs count. Therefore, ClassSR slows down model inference speed. In contrast, inserting our FourierSR allows methods to reduce model depth or width, thus reducing computational costs and speeding up model inference. Therefore, we can draw that our FourierSR provide a solution to further reduce network complexity while maintain the SR performance.

D. Ablation Study

1) *Theoretical Validity*: We demonstrate whether the theory of FourierSR holds in two cases. **First**: Is the PSNR gain due to increased computational costs? As shown in TABLE V, we compare existing methods in TABLE III inserted with our

Table VI: Ablation study on components of FourierSR shown in Fig. 2 on Manga109 [6] test set at a scale of $\times 2$.

Methods	Channel Tokens Mix	Real Part	Imag Part	Upper Branch	Lower Branch	Params↓	FLOPs↓	PSNR	SSIM
w/o CTM	✗	✓	✓	✓	✓	1378K	324.6G	38.72 _{-0.17}	0.9772 _{-0.0003}
w/o Real	✓	✗	✓	✓	✓	1382K	326.5G	38.75 _{-0.14}	0.9771 _{-0.0004}
w/o Imag	✓	✓	✗	✓	✓	1382K	326.5G	38.77 _{-0.12}	0.9771 _{-0.0004}
w/o Upper	✓	✓	✓	✗	✓	1382K	326.5G	38.78 _{-0.11}	0.9772 _{-0.0003}
w/o Lower	✓	✓	✓	✓	✗	1382K	326.5G	38.76 _{-0.13}	0.9771 _{-0.0004}
EDSR-Ours	✓	✓	✓	✓	✓	1384K	326.5G	38.89	0.9775

Table VII: Ablation study on the impact of the number of channel token mixes (CTM) in our FourierSR.

Scale	Methods	Params↓	FLOPs↓	Manga109 [6]
				PSNR/SSIM
$\times 2$	EDSR-Ours (0CTM)	1373K	324.6G	38.72/0.9772
	EDSR-Ours (1CTM)	1384K	326.5G	38.89 _{+0.17} /0.9775
	EDSR-Ours (2CTM)	1392K	328.4G	38.92 _{+0.20} /0.9775
	EDSR-Ours (4CTM)	1409K	332.2G	38.94 _{+0.22} /0.9775
	EDSR-Ours (8CTM)	1442K	339.4G	38.90 _{+0.18} /0.9774

FourierSR and a larger size version of these methods, where FourierSR performs much better in PSNR values due to its ability to capture global receptive fields. Additionally, due to the extremely lightweight nature of our FourierSR, it has a much lower number of parameters and FLOPs than the large-size version of these methods at a reasonable inference speed. Next, we show a visualization of feature maps at the same depth under different models in Fig. 8. Models can enhance the sharpness of high-frequency regions in feature maps by increasing computational costs, but the improvement is limited. In contrast, our FourierSR is more effective in recovering a clear high-frequency feature map. **Second:** Is the PSNR gain due to the convolution theorem? As shown in Fig. 9, we remove the Fourier transform (FFT) and inverse Fourier transform (IFFT) to disallow the convolution theorem, resulting in extremely limited PSNR gains caused by the inability to model global convolution. These two parts of ablation studies illustrate that the improved performance is not due to the increased computational cost of our FourierSR but rather to the successful simulation of global convolution.

2) *Modular Components:* As shown in TABLE VI, we verify the effectiveness of modular components in our FourierSR. First, we show the effectiveness of the channel token mix (CTM) in FourierSR in the first row, in which CTM greatly enhances the model representation by exchanging information on different channel tokens, achieving a PSNR gain of 0.17dB at the cost of increasing the number of parameters by only 4K and FLOPs by only 2.1G. Additionally, as shown in TABLE VII, we explain why we use one channel token mix (CTM) in our FourierSR. This is because the performance gain is insignificant when using more than 1 CTM in FourierSR. From the perspective of model efficiency, we insert 1 CTM in FourierSR from an efficiency point of view.

Then, we explain the importance of utilizing the Fourier features' real and imaginary parts separately in FourierSR, which has been proven in reasoning that can enhance the global receptive field of models. As shown in the second and third rows

Table VIII: Comparison of our FourierSR with (**Top**) Convolutional Neural Network (CNN) [29], windows-based Transformer (WTrans) [50], and (**Bottom**) existing token mix-based methods [13], [15]–[17], [31], [63].

Scale	Methods	Speed↓	Params↓	FLOPs↓	Manga109 [6]
					PSNR/SSIM
$\times 2$	EDSR	30ms	1370K	316.2G	38.55/0.9769
	EDSR-CNN [29]	81ms	2063K	456.6G	38.68/0.9772
	EDSR-WTrans [50]	162ms	1819K	404.7G	38.72/0.9773
	EDSR-GFNet [16]	155ms	30.8M	326.6G	38.70/0.9771
	EDSR-AFNO [13]	134ms	1472K	329.4G	38.83/0.9773
	EDSR-FFC [17]	76ms	1502K	363.2G	38.65/0.9771
	EDSR-AFFNet [15]	146ms	1574K	342.6G	NAN/NAN
	EDSR-FourierGNN [34]	181ms	1523K	336.1G	38.72/0.9772
	EDSR-DMixer [63]	122ms	1622K	386.1G	38.64/0.9770
	EDSR-Ours	58ms	1384K	326.5G	38.89/0.9775

of TABLE VI, this operator leads to an average PSNR increase of 0.13 dB while only growing the number of Params by 2K. Furthermore, as shown in Fig. 8, we visualize the upper and lower branches of FourierSR separately. Removing the upper branch (real part) reduces large-scale, low-frequency structures, while removing the lower branch (imag part) diminishes high-frequency details and edges, resulting in a less clear feature map. Next, we verify the effectiveness of adding and subbing the upper and lower branches to expand the receptive field theoretically. Similarly, as shown in the fourth and fifth rows of TABLE VI, this operator increases the PSNR by an average of 0.12 dB with only a 2K increase in the number of parameters, which fully illustrates the lightweight of such an operation and its ability to enhance global receptive fields effectively.

3) *Rationality of Designs:* **First**, as shown in the top of TABLE VIII, we compare our FourierSR with CNN [29] and Transformer [50], where CNN has limited performance gains, and the Transformer severely impacts model inference speeds. In contrast, our FourierSR is a better feature-extracting unit, which can further improve SR performance with fewer Params and FLOPs counts at a suitable inference speed. **Second**, as shown in the bottom of TABLE VIII, we show that our FourierSR design is more suitable for efficient SR than existing Fourier token-based methods. GFNet [16] defines global filters of the same size as the feature map as convolution kernels lead to huge parameter counts. The use of excessive matrix multiplications and built-in convolutions in AFNO [13], FFC [17], FourierGNN [34], and DMixer [63] significantly impacts the model's inference speed and computational cost. AFFNet [15] defines Fourier features as global convolution kernels, leading to gradient explosion in SR. In contrast, our FourierSR improves SR the most and incurs a small cost.

Table IX: Comparison of the inference speed, Params counts, and FLOPs counts for a 3×3 convolution, a windows-based Transformer, and a FourierSR, where the convolutional kernel size is 3 and the number of channels is 64.

Scale	Modules	3×3 Conv	windows-based Trans	FourierSR
$\times 2$	Latency↓	0.4ms	517ms	2.0ms
	Params↓	36.864K	16.384K	0.896K
	FLOPs↓	8.493G	5.662G	0.644G

V. LIMITATION AND FUTURE WORK

Since the presence of the Fast Fourier Transform (FFT) and Inverse Fast Fourier Transform (IFFT) within our FourierSR affects the model’s inference speed to a certain extent, our FourierSR is suited to be used as a plug-in to incorporate into existing methods under certain quantitative constraints, rather than on a large scale. This ensures that methods empowered by our FourierSR maintain a reasonable inference speed while improving the model representation.

Specifically, comparing the 3×3 convolution and windows-based Transformer, the strength of our FourierSR lies in its lightweight nature with powerful representation capabilities, as can be seen from Param’s counts and FLOPs counts comparisons in TABLE IX, and performance comparisons in TABLE VIII. However, according to the latency comparison of TABLE IX, although our FourierSR has a huge advantage in inference speed compared to the windows-based Transformer, the inference speed advantage over the 3×3 convolution is insignificant. Therefore, when FourierSR is used on a large scale as a feature enhancement module in existing methods, inference speed will be slower than CNN-based models.

Inspired by sparse-based and window-based works that aim to reduce complexity, we will leverage sparse representations and window divisions in the future to further reduce the complexity of FFT and IFFT, thereby accelerating the inference of FourierSR while maintaining the ability to boost SR. Furthermore, the all-in-one restoration [1] builds a unified framework capable of handling multiple low-level tasks, including adverse weather restoration [64], [65], SR [40], and deblur [32]. Our FourierSR exhibits potential owing to its plug-and-play nature, which we plan to further explore.

VI. CONCLUSION

This paper proposes FourierSR, a plugin to uniformly improve off-the-shelf efficient SR methods with low computational costs and global receptive fields. To achieve this goal, motivated by the token mix and the convolution theorem, real or imaginary parts of the Fourier domain features perform the token mix with global filters obtained by expanding our defined local filters. We demonstrate that the above operations are mathematically equivalent to performing global convolutions on the input plus the inverse of the input, avoiding the instability or inefficiency in existing token mixes. Experiments show that incorporating FourierSR into existing methods can significantly extend its receptive field, significantly improving efficient SR performance with a minimal computational cost.

REFERENCES

- [1] J. Jiang, Z. Zuo, G. Wu, K. Jiang, and X. Liu, “A survey on all-in-one image restoration: Taxonomy, evaluation and future trends,” *IEEE Transactions on Pattern Analysis and Machine Intelligence*, 2025.
- [2] W. Li, M. Wang, K. Zhang, J. Li, X. Li, Y. Zhang, G. Gao, and Z. Ma, “Survey on deep face restoration: From non-blind to blind and beyond,” *ACM Computing Surveys*, 2025.
- [3] Z. Hui, X. Gao, Y. Yang, and X. Wang, “Lightweight image super-resolution with information multi-distillation network,” in *ACMMM*, 2019, pp. 2024–2032.
- [4] G. Gao, W. Li, J. Li, F. Wu, H. Lu, and Y. Yu, “Feature distillation interaction weighting network for lightweight image super-resolution,” in *AAAI*, vol. 36, no. 1, 2022, pp. 661–669.
- [5] J. Liang, J. Cao, G. Sun, K. Zhang, L. Van Gool, and R. Timofte, “Swinir: Image restoration using swin transformer,” in *ICCVW*, 2021, pp. 1833–1844.
- [6] Y. Matsui, K. Ito, Y. Aramaki, A. Fujimoto, T. Ogawa, T. Yamasaki, and K. Aizawa, “Sketch-based manga retrieval using manga109 dataset,” *Multimedia Tools and Applications*, vol. 76, pp. 21 811–21 838, 2017.
- [7] W. Luo, Y. Li, R. Urtasun, and R. Zemel, “Understanding the effective receptive field in deep convolutional neural networks,” in *NeurIPS*, vol. 29, 2016.
- [8] B. Lim, S. Son, H. Kim, S. Nah, and K. Mu Lee, “Enhanced deep residual networks for single image super-resolution,” in *CVPRW*, 2017, pp. 136–144.
- [9] N. Ahn, B. Kang, K.-A. Sohn, and K.-A. Sohn, “Fast, accurate, and lightweight super-resolution with cascading residual network,” in *ECCV*, 2018, pp. 252–268.
- [10] G. Gao, Z. Wang, J. Li, W. Li, Y. Yu, and T. Zeng, “Lightweight bimodal network for single-image super-resolution via symmetric cnn and recursive transformer,” in *IJCAI*, 2022, pp. 913–919.
- [11] A. V. Oppenheim, *Discrete-time signal processing*. Pearson Education India, 1999.
- [12] Z. Li, N. Kovachki, K. Azizzadenesheli, B. Liu, K. Bhattacharya, A. Stuart, and A. Anandkumar, “Fourier neural operator for parametric partial differential equations,” in *ICLR*, 2021.
- [13] J. Guibas, M. Mardani, Z. Li, A. Tao, A. Anandkumar, and B. Catanzaro, “Efficient token mixing for transformers via adaptive fourier neural operators,” in *ICLR*, 2022.
- [14] Z. Liu, Y. Lin, Y. Cao, H. Hu, Y. Wei, Z. Zhang, S. Lin, and B. Guo, “Swin transformer: Hierarchical vision transformer using shifted windows,” in *ICCV*, 2021, pp. 10 012–10 022.
- [15] Z. Zhang, Z. Zhang, C. Lan, Z.-J. Zha, Y. Lu, and B. Guo, “Adaptive frequency filters as efficient global token mixers,” in *ICCV*, 2023, pp. 6049–6059.
- [16] Y. Rao, W. Zhao, Z. Zhu, J. Lu, and J. Zhou, “Global filter networks for image classification,” in *NeurIPS*, vol. 34, 2021, pp. 980–993.
- [17] L. Chi, B. Jiang, and Y. Mu, “Fast fourier convolution,” in *NeurIPS*, vol. 33, 2020, pp. 4479–4488.
- [18] J. Li, F. Fang, K. Mei, and G. Zhang, “Multi-scale residual network for image super-resolution,” in *ECCV*, 2018, pp. 517–532.
- [19] Z. Zhang, X. Wang, and C. Jung, “Dcsr: Dilated convolutions for single image super-resolution,” *IEEE Transactions on Image Processing*, vol. 28, no. 4, pp. 1625–1635, 2018.
- [20] F. Fang, J. Li, and T. Zeng, “Soft-edge assisted network for single image super-resolution,” *IEEE Transactions on Image Processing*, vol. 29, pp. 4656–4668, 2020.
- [21] Q. Cai, Y. Qian, J. Li, J. Lyu, Y.-H. Yang, F. Wu, and D. Zhang, “Hipa: hierarchical patch transformer for single image super resolution,” *IEEE Transactions on Image Processing*, vol. 32, pp. 3226–3237, 2023.
- [22] J. Li, Z. Pei, W. Li, G. Gao, L. Wang, Y. Wang, and T. Zeng, “A systematic survey of deep learning-based single-image super-resolution,” *ACM Computing Surveys*, vol. 56, no. 10, pp. 1–40, 2024.
- [23] B. Li, B. Wang, J. Liu, Z. Qi, and Y. Shi, “s-lwsr: Super lightweight super-resolution network,” *IEEE Transactions on Image Processing*, vol. 29, pp. 8368–8380, 2020.
- [24] Z. Hui, X. Wang, and X. Gao, “Fast and accurate single image super-resolution via information distillation network,” in *CVPR*, 2018, pp. 723–731.
- [25] J. Liu, J. Tang, and G. Wu, “Residual feature distillation network for lightweight image super-resolution,” in *ECCVW*. Springer, 2020, pp. 41–55.
- [26] W. Li, J. Li, G. Gao, W. Deng, J. Yang, G.-J. Qi, and C.-W. Lin, “Efficient image super-resolution with feature interaction weighted hybrid network,” *IEEE Transactions on Multimedia*, 2024.

- [27] L. Sun, J. Pan, and J. Tang, "Shufflemixer: An efficient convnet for image super-resolution," in *NeurIPS*, vol. 35, 2022, pp. 17 314–17 326.
- [28] G. Wu, J. Jiang, J. Jiang, and X. Liu, "Transforming image super-resolution: a convformer-based efficient approach," *IEEE Transactions on Image Processing*, vol. 33, pp. 6071–6082, 2024.
- [29] M. Zheng, L. Sun, J. Dong, and J. Pan, "Smfanet: A lightweight self-modulation feature aggregation network for efficient image super-resolution," in *ECCV*. Springer, 2025, pp. 359–375.
- [30] A. K. Sinha, S. M. Moorthi, and D. Dhar, "NI-ffc: Non-local fast fourier convolution for image super resolution," in *CVPRW*, 2022, pp. 467–476.
- [31] Y. Tatsunami and M. Taki, "Fft-based dynamic token mixer for vision," in *AAAI*, vol. 38, no. 14, 2024, pp. 15 328–15 336.
- [32] L. Kong, J. Dong, J. Ge, M. Li, and J. Pan, "Efficient frequency domain-based transformers for high-quality image deblurring," in *CVPR*, 2023, pp. 5886–5895.
- [33] J. Lee-Thorp, J. Ainslie, I. Eckstein, and S. Ontanon, "Fnet: Mixing tokens with fourier transforms," in *NAACL*, 2021.
- [34] K. Yi, Q. Zhang, W. Fan, H. He, L. Hu, P. Wang, N. An, L. Cao, and Z. Niu, "Fouriergnn: Rethinking multivariate time series forecasting from a pure graph perspective," in *NeurIPS*, vol. 36, 2024.
- [35] Z. Lu, J. Li, H. Liu, C. Huang, L. Zhang, and T. Zeng, "Transformer for single image super-resolution," in *CVPR*, 2022, pp. 457–466.
- [36] X. Zhang, H. Zeng, S. Guo, and L. Zhang, "Efficient long-range attention network for image super-resolution," in *ECCV*. Springer, 2022, pp. 649–667.
- [37] H. Wang, X. Chen, B. Ni, Y. Liu, and J. Liu, "Omni aggregation networks for lightweight image super-resolution," in *CVPR*, 2023, pp. 22 378–22 387.
- [38] W. Li, H. Guo, X. Liu, K. Liang, J. Hu, Z. Ma, and J. Guo, "Efficient face super-resolution via wavelet-based feature enhancement network," in *ACM MM*, 2024, pp. 4515–4523.
- [39] W. Li, H. Guo, Y. Hou, G. Gao, and Z. Ma, "Dual-domain modulation network for lightweight image super-resolution," *IEEE Transactions on Multimedia*, 2025.
- [40] W. Li, J. Li, G. Gao, W. Deng, J. Zhou, J. Yang, and G.-J. Qi, "Cross-receptive focused inference network for lightweight image super-resolution," *IEEE Transactions on Multimedia*, vol. 26, pp. 864–877, 2023.
- [41] H. Choi, J. Lee, and J. Yang, "N-gram in swin transformers for efficient lightweight image super-resolution," in *CVPR*, 2023, pp. 2071–2081.
- [42] Y. Zhou, Z. Li, C.-L. Guo, S. Bai, M.-M. Cheng, and Q. Hou, "Srformer: Permuted self-attention for single image super-resolution," in *ICCV*, 2023, pp. 12 780–12 791.
- [43] H. Guo, J. Li, T. Dai, Z. Ouyang, X. Ren, and S.-T. Xia, "Mambair: A simple baseline for image restoration with state-space model," in *ECCV*, 2024.
- [44] C. Wang, J. Jiang, Z. Zhong, and X. Liu, "Spatial-frequency mutual learning for face super-resolution," in *CVPR*, 2023, pp. 22 356–22 366.
- [45] J. Huang, Y. Liu, F. Zhao, K. Yan, J. Zhang, Y. Huang, M. Zhou, and Z. Xiong, "Deep fourier-based exposure correction network with spatial-frequency interaction," in *ECCV*. Springer, 2022, pp. 163–180.
- [46] H. Yu, N. Zheng, M. Zhou, J. Huang, Z. Xiao, and F. Zhao, "Frequency and spatial dual guidance for image dehazing," in *ECCV*. Springer, 2022, pp. 181–198.
- [47] C. Wang, H. Wu, and Z. Jin, "Fourllie: Boosting low-light image enhancement by fourier frequency information," in *ACM MM*, 2023, pp. 7459–7469.
- [48] X. Lv, S. Zhang, C. Wang, Y. Zheng, B. Zhong, C. Li, and L. Nie, "Fourier priors-guided diffusion for zero-shot joint low-light enhancement and deblurring," in *CVPR*, 2024, pp. 25 378–25 388.
- [49] Z. Zou, H. Yu, J. Huang, and F. Zhao, "Freqmamba: Viewing mamba from a frequency perspective for image deraining," in *ACM MM*, 2024, pp. 1905–1914.
- [50] X. Liu, J. Liu, J. Tang, and G. Wu, "Catanet: Efficient content-aware token aggregation for lightweight image super-resolution," in *CVPR*, 2025, pp. 17 902–17 912.
- [51] M. Bevilacqua, A. Roumy, C. Guillemot, and M. L. Alberi-Morel, "Low-complexity single-image super-resolution based on nonnegative neighbor embedding," in *BMVC*, vol. 135, 2012, pp. 1–10.
- [52] R. Zeyde, M. Elad, and M. Protter, "On single image scale-up using sparse-representations," in *JCCS*. Springer, 2012, pp. 711–730.
- [53] D. Martin, C. Fowlkes, D. Tal, and J. Malik, "A database of human segmented natural images and its application to evaluating segmentation algorithms and measuring ecological statistics," in *ICCV*, vol. 2. IEEE, 2001, pp. 416–423.
- [54] J.-B. Huang, A. Singh, and N. Ahuja, "Single image super-resolution from transformed self-exemplars," in *CVPR*, 2015, pp. 5197–5206.
- [55] X. Kong, H. Zhao, Y. Qiao, and C. Dong, "Classsr: A general framework to accelerate super-resolution networks by data characteristic," in *CVPR*, 2021, pp. 12 016–12 025.
- [56] S. Gu, A. Lugmayr, M. Danelljan, M. Fritsche, J. Lamour, and R. Timofte, "Div8k: Diverse 8k resolution image dataset," in *ICCVW*. IEEE, 2019, pp. 3512–3516.
- [57] C. Dong, C. C. Loy, and X. Tang, "Accelerating the super-resolution convolutional neural network," in *ECCV*. Springer, 2016, pp. 391–407.
- [58] C. Ledig, L. Theis, F. Huszár, J. Caballero, A. Cunningham, A. Acosta, A. Aitken, A. Tejani, J. Totz, Z. Wang *et al.*, "Photo-realistic single image super-resolution using a generative adversarial network," in *CVPR*, 2017, pp. 4681–4690.
- [59] X. Zhang, Y. Zhang, and F. Yu, "Hit-sr: Hierarchical transformer for efficient image super-resolution," in *ECCV*. Springer, 2024, pp. 483–500.
- [60] H. Guo, Y. Guo, Y. Zha, Y. Zhang, W. Li, T. Dai, S.-T. Xia, and Y. Li, "Mambairv2: Attentive state space restoration," in *CVPR*, 2025, pp. 28 124–28 133.
- [61] R. Timofte, E. Agustsson, L. Van Gool, M.-H. Yang, and L. Zhang, "Ntire 2017 challenge on single image super-resolution: Methods and results," in *CVPRW*, 2017, pp. 114–125.
- [62] Z. Wang and A. C. Bovik, "A universal image quality index," *IEEE Signal Processing Letters*, vol. 9, no. 3, pp. 81–84, 2002.
- [63] M. Lou, S. Zhang, H.-Y. Zhou, S. Yang, C. Wu, and Y. Yu, "Transxnet: learning both global and local dynamics with a dual dynamic token mixer for visual recognition," *IEEE Transactions on Neural Networks and Learning Systems*, 2025.
- [64] S. Sun, W. Ren, X. Gao, R. Wang, and X. Cao, "Restoring images in adverse weather conditions via histogram transformer," in *ECCV*. Springer, 2024, pp. 111–129.
- [65] W. Li, J. Shi, J. Han, H. Guo, and Z. Ma, "Seeing through the rain: Resolving high-frequency conflicts in deraining and super-resolution via diffusion guidance," in *AAAI*, 2026.